

Developing versus Nondeveloping Disturbances for Tropical Cyclone Formation. Part I: North Atlantic*

MELINDA S. PENG

Marine Meteorology Division, Naval Research Laboratory, Monterey, California

BING FU

International Pacific Research Center, University of Hawaii at Manoa, Honolulu, Hawaii

TIM LI

International Pacific Research Center, and Department of Meteorology, University of Hawaii at Manoa, Honolulu, Hawaii

DUANE E. STEVENS

Department of Meteorology, University of Hawaii at Manoa, Honolulu, Hawaii

(Manuscript received 9 September 2010, in final form 13 September 2011)

ABSTRACT

This study investigates the characteristic differences of tropical disturbances that eventually develop into tropical cyclones (TCs) versus those that did not, using global daily analysis fields of the Navy Operational Global Atmospheric Prediction System (NOGAPS) from the years 2003 to 2008. Time filtering is applied to the data to extract tropical waves with different frequencies. Waves with a 3–8-day period represent the synoptic-scale disturbances that are representatives as precursors of TCs, and waves with periods greater than 20 days represent the large-scale background environmental flow. Composites are made for the developing and nondeveloping synoptic-scale disturbances in a Lagrangian frame following the disturbances. Similarities and differences between them are analyzed to understand the dynamics and thermodynamics of TC genesis. Part I of this study focuses on events in the North Atlantic, while Part II focuses on the western North Pacific.

A box difference index (BDI), accounting for both the mean and variability of the individual sample, is introduced to subjectively and quantitatively identify controlling parameters measuring the differences between developing and nondeveloping disturbances. Larger amplitude of the BDI implies a greater possibility to differentiate the difference between two groups. Based on their BDI values, the following parameters are identified as the best predictors for cyclogenesis in the North Atlantic, in the order of importance: 1) water vapor content within 925 and 400 hPa, 2) rain rate, 3) sea surface temperature (SST), 4) 700-hPa maximum relative vorticity, 5) 1000–600-hPa vertical shear, 6) translational speed, and 7) vertically averaged horizontal shear. This list identifies thermodynamic variables as more important controlling parameters than dynamic variables for TC genesis in the North Atlantic. When the east and west (separated by 40°W) Atlantic are examined separately, the 925–400-hPa water vapor content remains as the most important parameter for both regions. The SST and maximum vorticity at 700 hPa have higher importance in the east Atlantic, while SST becomes less important and the vertically averaged horizontal shear and horizontal divergence become more important in the west Atlantic.

* School of Ocean and Earth Science and Technology Contribution Number 8553 and International Pacific Research Center Contribution Number 852.

Corresponding author address: Tim Li, International Pacific Research Center, 1680 East-West Rd., POST 409B, Honolulu, HI 96822.
E-mail: timli@hawaii.edu

1. Introduction

Tropical cyclone (TC) genesis remains one of the least understood phenomena in atmospheric science because of the multiple-scale interactions involved and lack of in situ observations over open oceans. Gray (1968, 1975) listed environmental conditions that are necessary or favorable for TC formation: sea surface temperature (SST) greater than 26.5°C, abundant low-to-midlevel moisture, substantial decrease of equivalent potential temperature from surface to midlevel, small vertical shear, large relative vorticity, and a location that is a few degrees latitude away from the equator.

Of the many tropical disturbances in global ocean basins, only a small fraction develops into TCs. For example, Fig. 1 shows the 3–8-day filtered relative vorticity in the time–longitude frame for 2004 and 2005 from 100°W to 10°E averaged in two latitudinal bands (5°–15°N for the year 2004 and 15°–25°N for the year 2005). Every 2 or 3 days, an organized synoptic-scale wave is generated on the African continent east of the prime meridian and propagates westward. These synoptic waves are identified as African easterly waves (AEWs) to denote their point of origin. Most hurricanes in the North Atlantic (NATL) form from the AEWs (Avila 1991; Avila and Pasch 1995; Landsea 1993). The red dots in Fig. 1 denote the longitude and time of TC genesis events based on the National Hurricane Center (NHC) best-track data. The majority of AEWs, though having significant low-level vorticity, did not form TCs. Avila (1991) found that about 58 tropical waves move across the Atlantic basin during the hurricane season per year, but only 30% of them develop into TCs. Landsea (1993) further pointed out that about 58% of the Atlantic tropical storms and 57% of the minor hurricanes (Saffir–Simpson scale categories 1 and 2) originate from easterly waves, and 83% of the intense/major (category 3 or above) hurricanes have their origins as AEWs. Earlier, most of the studies on TC formation associated with AEWs relied mainly on satellite images and/or rawinsonde observations. Carlson (1969) identified three easterly waves within 2 weeks that eventually developed into Atlantic TCs. Simpson et al. (1968) investigated Atlantic tropical disturbances during the 1967 hurricane season and pointed out that about 50% of the 61 disturbances are associated with the AEWs. Erickson (1977) concluded that there are no apparent differences in the overall amount and intensity of convective cloudiness between nondeveloping cloud clusters and prestorm disturbances.

McBride and Zehr (1981) analyzed 912 different tropical systems using rawinsonde data. Their composite results show many common features between developing and nondeveloping systems in the NATL. Both types

have an upper-level warm core, a similar horizontal moisture structure, and hardly distinguishable temperature and moisture gradients. However, the developing disturbances usually possess greater cyclonic winds in the lower level and greater anticyclonic winds in the upper level than the nondeveloping disturbances; also, the nondeveloping systems show weaker vertical motions.

With the advancement of remote sensing technology, more Atlantic storms are identified as being generated within the AEWs (Landsea et al. 1998). In addition, significant improvement in the quality of global atmospheric analysis has been achieved through improvements in satellite retrieval, data assimilation, and numerical modeling. Thorncroft and Hodges (2001) tracked vorticity centers in the European Centre for Medium-Range Weather Forecasts (ECMWF) analyses and found a positive correlation between the AEWs activities south of 15°N and the Atlantic TC activities. However, as they suggested, the results are not conclusive because of their short-period data analysis. Hopsch et al. (2007) extended Thorncroft and Hodges' studies and found that the positive correlation between AEWs and Atlantic TC activities is not significant. DeMaria et al. (2001) proposed a genesis parameter for the TCs in the NATL. This parameter is the product of appropriately scaled 5-day running mean vertical shear, instability, and midlevel moisture variables. The instability and shear variables are calculated from operational National Centers for Environmental Prediction (NCEP) analyses, and the midlevel moisture variable is determined from cloud-clear Geostationary Operational Environmental Satellite (GOES) water vapor imagery. Because this parameter only reflects the properties of a geographically fixed environment, it actually provides an evaluation of the potential for TC genesis.

Frank and Roundy (2006) analyzed relationships between tropical wave activity and tropical cyclogenesis in major TC basins. Mixed Rossby–gravity waves, tropical-depression-type or easterly waves, equatorial Rossby waves, Kelvin waves, and the Madden–Julian oscillation were examined. TC formation is closely related to enhanced activity in these filtered wave bands except for the Kelvin wave. In each basin, the structure of each composite wave and the phase relationship between the wave and cyclogenesis are similar, suggesting consistent forcing mechanisms. The waves appear to enhance the local circulations by increasing the forced upward vertical motion, increasing low-level vorticity, and modulating the vertical shear. Convective anomalies of waves associated with genesis are detectable in the analyses as long as 1 month prior to genesis. This finding opens up the possibility of developing a statistically based TC genesis forecast model.

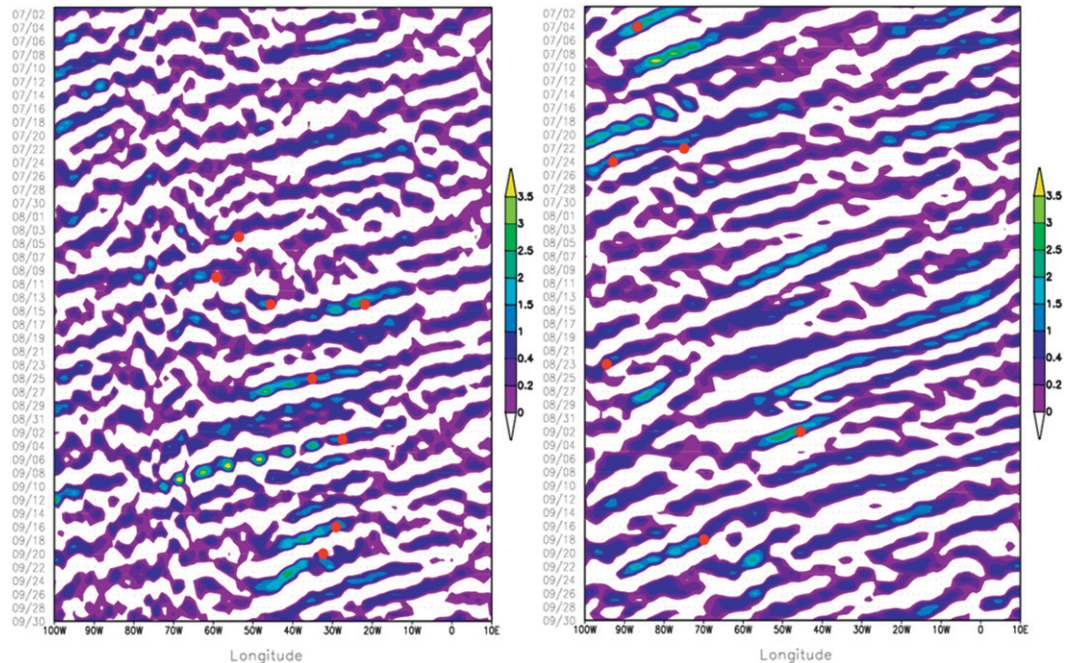


FIG. 1. Time-longitude profile of NOGAPS 3–8-day filtered 850-hPa relative vorticity (10^{-5} s^{-1}) between (left) 5° and 15°N in 2004 and (right) 15° and 25°N in 2005. The red dots represent TC genesis longitude–time.

Most recently, Hopsch et al. (2010) compared the structure of AEWs with 40-yr ECMWF Re-Analysis (ERA-40) data and found the nondeveloping and developing composites have similar evolutions before reaching the western African coast, except that the amplitudes of nondeveloping waves are weaker and there is less convective activity in the Guinea Highlands region. The nondeveloping AEW also shows a more prominent dry signal just ahead of the AEW trough at mid- to upper levels. Braun (2010) reevaluated the role played by the Saharan air layer (SAL) in Atlantic tropical cyclone genesis and suggested the negative influence of SAL on tropical cyclone genesis has perhaps been overemphasized in the research community.

Burpee (1972) indicated that AEWs were generated via barotropic and/or baroclinic instability associated with the African easterly jet (AEJ) and AEWs usually develop equatorward of the jet core where the mean flow is dynamically unstable. This idea was supported and well accepted in many studies that followed (Rennick 1976; Simmons 1977; Thorncroft and Hoskins 1994a,b; Paradis et al. 1995). Based on a July–September 2004 analysis, Berry et al. (2007) identified that AEWs mature over the African continent with structure ranging from isolated potential vorticity maxima confined equatorward of the objectively defined African easterly jet to broad cross-jet structures symptomatic of both baroclinic and barotropic growth. After leaving the West African coast,

45% of the AEWs in the July–September 2004 period were associated with tropical cyclogenesis. However, Hall et al. (2006) suggested that the hydrodynamic instability of the mean flow may be too weak for easterly waves to amplify at a realistic time scale. Thorncroft et al. (2008) recently pointed out that the AEJ is too short to support the sufficient growth of the AEWs and thus cannot explain the observed amplitude of the AEWs in West Africa. They argued that AEWs are triggered and maintained by localized forcing, most likely associated with latent heating upstream of the observed AEW growth region.

In this study, we use global daily analysis data to investigate different characteristics associated with tropical disturbances that eventually formed TCs and those that did not. Recent improvements in numerical models, assimilation of satellite data, and data assimilation schemes have led to great improvement in numerical model performance, in part reflected by the prediction of TC tracks (Franklin 2008). These advancements also led to an improvement in the quality of the analysis fields.

Part I of this study reports the findings for the NATL and Fu et al. (2012, hereafter Part II) looks at the western North Pacific (WNP). Part II also includes comparison between the two basins. Studies for tropical disturbances in the other regions such as the eastern Pacific, Indian Ocean, and Australia will be carried out in future studies. Section 2 describes the data and methodology used to identify developing and nondeveloping

tropical disturbances. The composite mean and variability of various key variables and parameters for these two groups of tropical disturbances are presented in section 3. In section 4, the relationship between the upstream easterly wind and downstream TC development is discussed. Summary and discussions are given in section 5.

2. Data and methodology

a. Data

The 1°-resolution daily global analysis of the Navy Operational Global Atmospheric Prediction System (NOGAPS) is treated as a proxy for the real atmosphere. Many studies have demonstrated the usefulness of global analyses in understanding various phenomena. This 1°-resolution dataset is sufficient for studying the characteristics of tropical synoptic disturbances. NOGAPS has four analyses (0000, 0600, 1200, and 1800 UTC) for each day; however, only the 0000 UTC data are used in this study. The data we examined cover the period from 2003¹ to 2008.

In addition to the NOGAPS analysis, the Tropical Rainfall Measuring Mission (TRMM) Microwave Imager (TMI) SST and the precipitation rate for the 6-yr period are also used in the study. TRMM is a joint mission supported by the National Aeronautics and Space Administration (NASA) and the National Space Development Agency of Japan (NSDAJ). TMI data cover the entire global tropical region 40°S–40°N. Besides SST and precipitation rate data, TRMM also provides surface wind speeds, atmospheric water vapor, and cloud liquid water with a horizontal resolution of $0.25^\circ \times 0.25^\circ$. These satellite products have been included in the data assimilation of the global analysis, but not used directly in the present study.

b. Filtering and case selection

A bandpass filtering technique (Christiano and Fitzgerald 2003) is applied to the daily analysis field to retrieve signals with a 3–8-day period, which are generally regarded as synoptic-scale disturbances that exist as precursors to TCs during the genesis stage (Wallace and Chang 1969; Lau and Lau 1990; Tam and Li 2006; Fu et al. 2007). The wavelengths of these waves are typically in the range of 2000–2500 km. A low-pass filter is applied to obtain lower-frequency variabilities with periods greater than 20 days that represent a large-scale environment, with a wavelength around 6000 km or greater.

TABLE 1. List of the number of developing and nondeveloping cases in July, August, and September in the NATL from 2003 to 2008.

	Developing				Nondeveloping			
	Jul	Aug	Sep	Tot	Jul	Aug	Sep	Tot
2003	4	4	5	13	6	4	5	15
2004	0	5	5	10	5	9	7	21
2005	5	6	6	17	6	5	8	19
2006	0	3	4	7	7	7	5	19
2007	0	3	4	7	6	5	5	16
2008	2	3	3	8	5	9	4	18
Tot	11	24	27	62	35	39	34	108

In this study, we define the disturbances of the NATL as those that are over the Atlantic and within a domain from the equator to 30°N and 100°W–10°E. The disturbances of the WNP are within a domain from the equator to 30°N and 100°E–160°W. Despite the fact that some TCs do occur beyond 30°N, they are not included because those disturbances are usually associated with midlatitude systems and their characteristics are quite different from tropical disturbances. For the NATL, we focus on disturbances that occurred from July to September, as previous studies have demonstrated that the AEWs peak during those 3 months (Grist 2002). In Part II, events from June to September are examined for the WNP.

First, the daily 3–8-day filtered 850-hPa wind and relative vorticity fields are examined to identify tropical disturbances. Two groups of disturbances are formed. The first group contains disturbances that formed TCs, identified by NHC in the NATL, or by the Joint Typhoon Warning Center (JTWC) in the WNP for Part II. Day 0 is designated as the day when a TC is first designated as a tropical depression (TD) with maximum sustained wind over 25 kt (12.9 m s^{-1}). We trace the disturbance 3 days back, designated as day -1 , -2 , and -3 . Note that NOGAPS includes synthetic data to enhance the structure of a cyclone when a system becomes a tropical storm; our identification of day 0 for developing cases is at the day before synthetic data are included (on day $+1$). In the study of the 1983/84 WNP TCs by Zehr (1992), the genesis period begins near the time of convective maximum and ends with the tropical storm designation. The average genesis period is 3.2 days. Based on Zehr's study, our tracking of 3 days back from the tropical storm stage is reasonable. There are 62 developing cases in the NATL from 2003 to 2008 (Table 1).²

¹ Some pressure level data for 2003 are not available for this study; in that case, we only use 5-yr data (2004–08).

² We exclude some TCs (Alex, Gaston, and Hermine) of 2004 as they either cannot be traced 3 days prior to formation or they are primarily associated with midlatitude frontal system.

In the WNP, 89 developing cases are selected (the corresponding table is shown in Part II).

Many of the nondeveloping disturbances lasted for a long period before they dissipated, while some dissipated within a few days. To identify those cases, we examined the 3–8-day filtered relative vorticity and wind fields. We defined three criteria for nondeveloping disturbances: 1) the mean radius of the cyclonic circulation is larger than 400 km, 2) the maximum of 3–8-day filtered relative vorticity is larger than 10^{-5} s^{-1} , and 3) the disturbance must satisfy criteria 1 and 2 for at least three consecutive days. The identification of the disturbances is carried out automatically with these criteria. By defining these criteria, we exclude weak and short-lived disturbances. Note that disturbances 3 days or more prior to TC formation for a developing case are not included in the nondeveloping cases. There are a total of 108 nondeveloping cases (Table 1) for 2003–08 in the NATL based on our analysis. For the WNP, 78 nondeveloping cases are selected (the corresponding table is shown in Part II).

Examples are shown to illustrate how the developing and nondeveloping disturbances are identified. For the developing cases, the task is straightforward, as cyclonic circulations can be identified clearly in the analysis based on the dates and locations of all TCs issued by NHC and JTWC. Once the day 0 disturbance is identified, we track backward in time following the disturbance to day -1 , -2 , and -3 using the filtered wind fields at 850 hPa. An example is given in Fig. 2a for Hurricane Frances identified by NHC as a tropical storm at 0000 UTC on 25 August 2004. The $20^\circ \times 20^\circ$ box in each diagram is centered on the disturbances at day 0, -1 , -2 , and -3 . An example of the nondeveloping disturbances is shown in Fig. 2b. The location of this disturbance is similar to that of the developing example shown in Fig. 2a. Comparing with the developing disturbance, the nondeveloping disturbance in Fig. 2b had a strong cyclonic circulation to start with, but dissipated later when it moved off the African coast. On the other hand, the disturbance in Fig. 2a for Frances had a very weak circulation while on the African continent but developed quickly once it moved to the ocean and formed Frances.

Once the developing and nondeveloping disturbances are identified, the analysis fields in a $20^\circ \times 20^\circ$ longitude–latitude box centered on the cyclonic circulation are examined to identify the differences in various parameters for the developing and nondeveloping groups, and to understand the dynamic and thermodynamic processes behind them. To achieve this goal, a composite is made for each day of the 4-day period (day -3 , -2 , -1 , and 0) for the developing group. For the nondeveloping disturbances, only one composite is made containing all individual vortices in the lifespan of all the nondeveloping disturbances.

3. Mean composites

a. Geographic distribution and translational speed

We computed the displacement vector of the developing and nondeveloping disturbances based on their locations on two consecutive days (Fig. 3a). For a developing disturbance, only the daily displacement vectors starting at day -3 , -2 , and -1 are displayed, as we do not look beyond day 0. For a nondeveloping disturbance, the vector at each day of its lifespan is shown. As most of these cyclonic disturbances are easterly waves originated in Africa, many of the nondeveloping disturbances died out or dissipated before reaching the central NATL; however, some of the dissipated disturbances later reintensified. Developing waves can travel well into the western NATL. The average translational speeds and standard deviations are shown in Fig. 3b. In general, the speeds of the developing disturbances tend to be slower as they reach tropical depression or tropical storm intensity. The averaged translational speed of the developing disturbances at day -1 is smaller than that of the nondeveloping disturbances, and the difference in the means of these two group samples is statistically significant at a 99% confidence level using a two-sample t test. As the translational speed of the disturbances in the NATL is closely related to the strength of the trade wind, this conclusion supports Frank's (1972) speculation that the likelihood of hurricanes occurring decreases in those years when the trades are abnormally strong. It is also consistent with an old empirical forecast rule stating that fast-moving disturbances rarely intensify. Figure 3a also clearly shows two separate tracks of the AEWs in the African continent and their merging after they move off the land, which is consistent with previous studies (e.g., Diedhiou et al. 1999). However, one needs to be cautious that the merging of tracks does not mean the merging of two vortices. Hopsch et al. (2007) noted that the merging of vorticity centers from two tracks is quite rare.

b. Horizontal pattern and evolution characteristics

In this section, we examine the horizontal patterns of some key meteorological variables and parameters to reveal the distinctive characteristics of the developing and nondeveloping disturbances. One aspect that is different from most previous studies is that we are following individual disturbances as they propagate instead of focusing on a geographically fixed region for TC genesis. Using the genesis-favorable list by Gray (1968, 1975) as a starting point, we make composites for the developing waves at day -3 , -2 , -1 , and 0. For the nondeveloping waves only one composite is made, which includes all the dates for all cases. Because the characteristics for the day -2 and -3 composites for

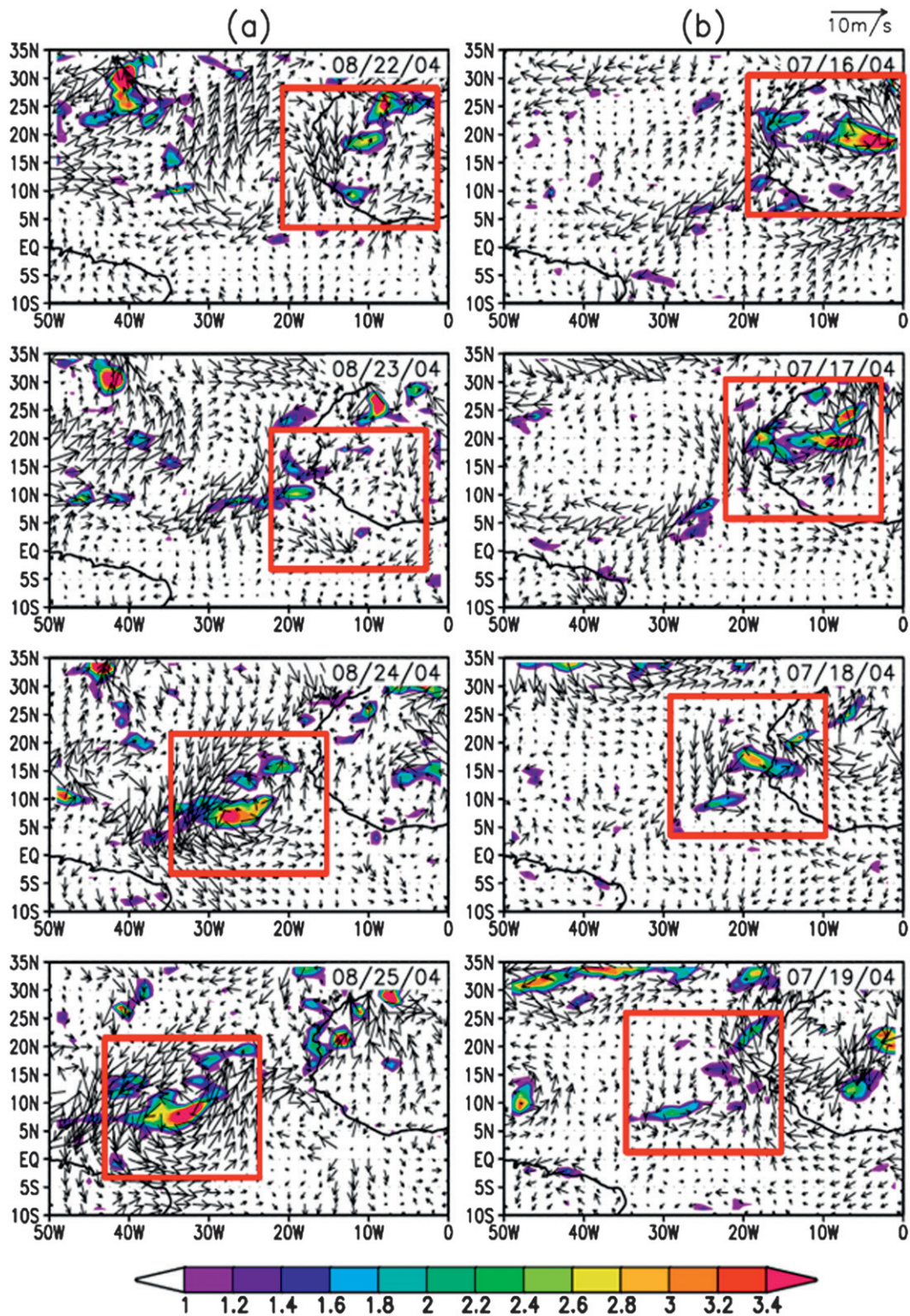


FIG. 2. NOGAPS 3–8-day filtered 850-hPa wind analysis (vectors) and relative vorticity (shading; 10^{-5} s^{-1}) on (a) 22–25 Aug 2004 and (b) 16–19 Jul 2004. In (a), red squares surround a developing wave, which became Hurricane Frances on 25 Aug. In (b), red squares surround a nondeveloping wave that eventually dissipated.

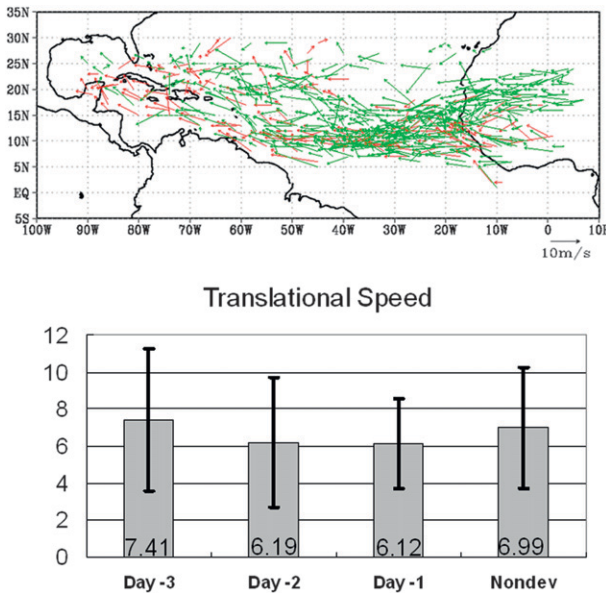


FIG. 3. (top) Daily displacement vectors of developing disturbances (red arrows) and nondeveloping disturbances (green arrows) in the NATL, and (bottom) average translational speed (bars) and corresponding standard deviation (whiskers). The value of average translational speed is marked at the bottom of each bar (m s^{-1}).

developing waves are in general very similar, we only display day -3, -1, and 0 composites for the developing waves along with the single composite for the nondeveloping cases.

The first variable examined is the 3–8-day filtered synoptic-scale relative vorticity field. We examine whether or not a composite pre-TC disturbance attained a higher relative vorticity than the composite nondeveloping disturbance. The composites of the 850- and 500-hPa relative vorticity of the 3–8-day filtered waves, depicted in Fig. 4a, do not show distinctively higher values of the relative vorticity for disturbances that eventually form TC. At day -3, the composite for the developing cases is weaker than the composite of all the nondeveloping cases. At day -2 (not shown) and day -1, they are slightly greater. Only at day 0, the relative vorticity for the developing disturbances is much larger than the composite for all the nondeveloping disturbances. By this time, as cyclogenesis will occur fairly soon (on average, within 12 h), its higher value may not be viewed as the pregenesis condition. If the composites for all the time frames of developing cases were made into a single one, as in the nondeveloping case, then the two groups would show very little difference. Thus, based on this analysis, we conclude that the developing disturbances do not possess stronger vorticity prior to their rapid development into a tropical storm compared to the nondeveloping disturbances. This implies that the formation process occurs rather quickly.

Note that the center of the maximum vorticity at 850 hPa lines up well with the center at 500 hPa for both the developing and the nondeveloping groups. This may reflect a strong vertical coupling in convective systems in the first-guess field as a result of the convective parameterization in NOGAPS (Peng et al. 2004), which may not necessarily be the true representative of the real atmosphere. The core region of the vorticity fields for both the developing and nondeveloping vortices are fairly symmetric at 850 and 500 hPa. The outer portion of the vortices for both the developing and nondeveloping disturbances shows some southwest–northeast tilt at 500 hPa.

Next we investigate SST, 500-hPa relative humidity, and rain-rate fields. No filtering is applied to these three fields. Figure 4b contains the SST composites. All four panels show a warm-tongue pattern with warm SST extending eastward. The domain averages SST for the developing waves at day -3, -1, and 0 are 27.94°, 28.20°, and 28.24°C, respectively, which exhibits a slight increasing trend as the time approaches the genesis date. The average SST for the nondeveloping disturbances is 27.53°C, which is lower than that for the developing waves. Thus the composite SST difference supports the notion that a warmer SST favors more TC genesis in the NATL. Note that the pattern for the developing disturbances—shown at day -3, -1, and 0—appears to be noisier than the nondeveloping group. This is mainly due to the sample size difference as the disturbances for developing group are subdivided into day -3, -2, -1, and 0, while the composite for the nondeveloping group includes all its individual ones. Therefore, the sample size for the developing ones at day -3, -2, -1, and 0 is roughly $\frac{1}{4}$ of the nondeveloping one. Another possibility is that noisier SST for developing disturbances may due to their feedback of more vigorous convective activities to the ocean SST.

Further examination of the climatological monthly-mean SST patterns shows that there are two warm SST tongues extending eastward in July (Fig. 5a). One is between 5° and 10°N, and the other is centered at 25°N. As shown in Fig. 3a, most of the disturbances are located over these two warm tongues. The September and July difference map (Fig. 5c) shows a general warming in the entire basin, with a maximum warming centered at 18°N, 21°W and extending southwestward. The Gulf of Mexico remains a warm basin throughout the season. The SST westward gradient is reflected by the composites shown in Fig. 4b for both the developing and nondeveloping groups. Consistent with the overall SST increase from July to September, the monthly distribution of the two groups given in Table 1 indicates that more disturbances are likely to develop into TCs in the late season, coinciding with increasing SST. The percentage

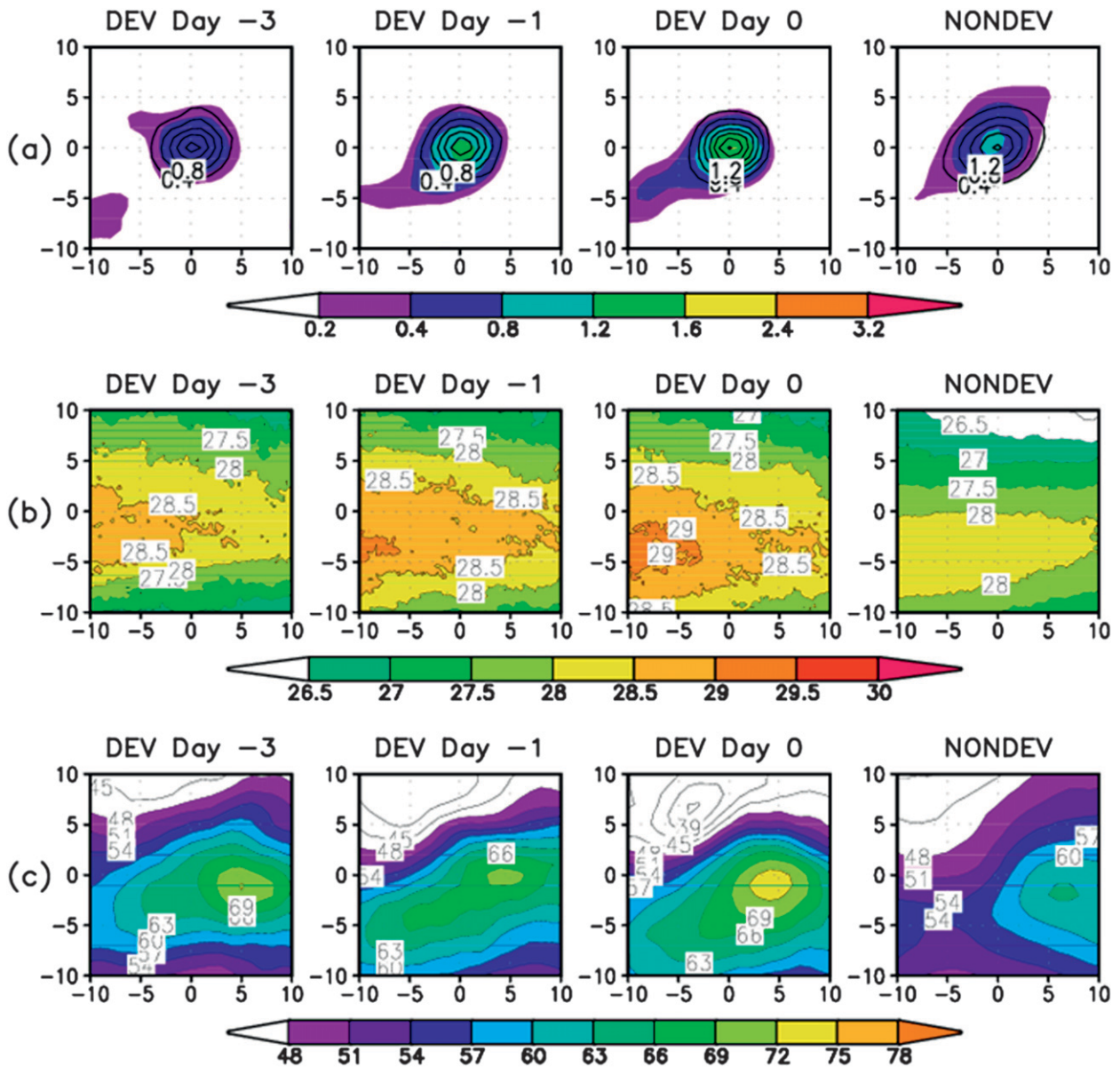


FIG. 4. Composite fields for developing and nondeveloping disturbances in the NATL. (a) 3–8-day filtered relative vorticity (10^{-5} s^{-1}) at 850 hPa (contours; interval = 0.4) and 500 hPa (shading), (b) SST ($^{\circ}\text{C}$), and (c) relative humidity at 500 hPa (%). For all the composite fields, the horizontal–vertical axis measures relative longitudinal–latitudinal distance in degrees from the center.

of the developing disturbances (relative to the total disturbances) is 24% in July, 38% in August, and 44% in September. This is consistent with the climatology of TC genesis in the Atlantic that peaks in September (Landsea 1993). Since most of the wave disturbances move westward toward warmer SST, it is not surprising that SST may be regarded as one of the primary environmental factors that determine the peak. Our composites reflect the role played by SST in TC formation.

The next parameter examined is the relative humidity at 500 hPa (Fig. 4c). The developing disturbances have

a distinctively higher relative humidity at 500 hPa than the nondeveloping waves. The maximum difference is about 10%. In both the developing and nondeveloping disturbance composites, drier air appears in the northern part of the vortex center, but the pattern is fairly symmetric to the vortex center in the north–south direction. As disturbances in the Atlantic are mostly easterly waves from Africa, the drier air to the north may originate from the Sahara Desert or midlatitudes (see section 5 for more discussion). The maximum humidity center is shifted to the east of the vorticity center. This

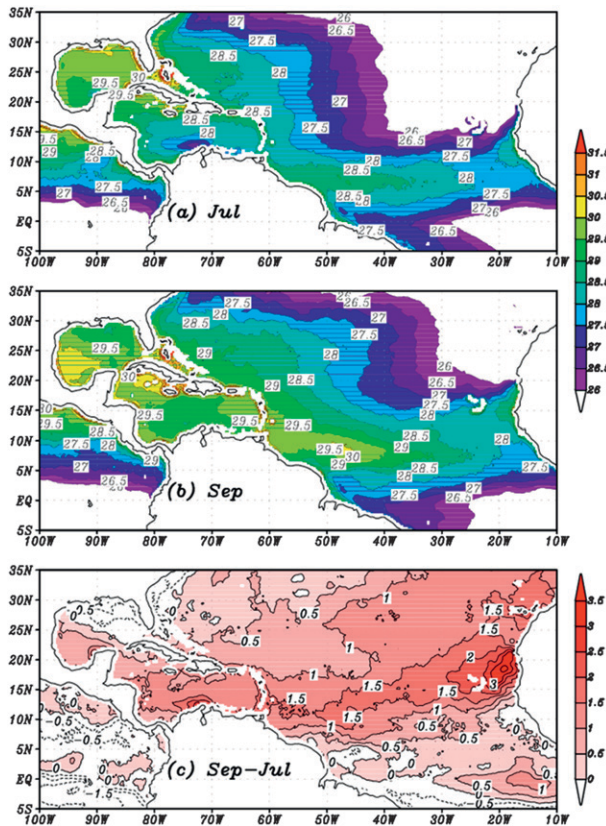


FIG. 5. Six-year (2003–08) mean TMI SST in the NATL in (a) July and (b) September and (c) difference between September and July ($^{\circ}\text{C}$).

phase shift is possibly a result of moist advection by southeasterly flows to the east of the easterly wave vortex maxima.

The rain-rate composite retrieved from the TMI data (Fig. 6a) corresponds well with the patterns of the relative humidity at 500 hPa. This is not surprising, as intense precipitation resulting from deep convection requires abundant moisture. Both local and domain-averaged rain rates for the developing disturbances, even at day -3 , are significantly greater than for the nondeveloping disturbances. In the developing cases, there are areas with intense precipitation but not in the nondeveloping waves. Hopsch et al. (2010) found that the lack of development of intense nondeveloping AEWs was due to the presence of dry mid- to upper-level air just ahead of the AEW trough. We did a composite for the strongest 62 nondeveloping AEWs and found a consistent result with Hopsch et al. (2010). It shows a very dry region just ahead of AEWs. However, unlike Hopsch et al.'s results, where intense nondeveloping AEWs exhibits strong convection activity, our composite of TMI rain rate for the strongest nondeveloping AEWs show significantly less rainfall than that of the developing

AEWs. The qualitative collocation between precipitation and relative humidity suggests that the moisture content associated with tropical disturbances plays an important role in their development into TCs. This, however, needs to be examined with other favorable conditions in the future.

Analysis of the IR brightness temperature (area where $\text{IR} < -65^{\circ}\text{C}$ within 4° radius) by Zehr (1992) showed that 80% of TCs in the WNP have an early convective maximum during the formation stage, typically 1–3 days before a tropical depression/storm is designated. In addition, there is a period of at least 24 h following the early convective maximum during which convection is significantly reduced. The average time interval between the early convective maximum and the first tropical storm designation is 3.2 days. The remaining 20% are characterized by a continuing increase in convection. Furthermore, many of the nondeveloping cases in Zehr's study have at least one convective maximum comparable in magnitude and duration to those typical of the pretropical storm cases for the WNP. Table 2 shows the duration of the nondeveloping disturbances in the NATL and the WNP. The duration period generally ranges from 3 to 11 days.

Figure 6b depicts the magnitude of the 200–850-hPa shear associated with time scales greater than 20 days, representing a large-scale atmospheric environment. The vertical shear is very similar between the developing group at day -3 and the nondeveloping group, but it decreases gradually at day -2 and -1 and decreases substantially at day 0 for developing waves. The detrimental effect of large environmental shear on the development of TCs has been well recognized (Gray 1975; Anthes 1982; DeMaria 1996). Strong vertical wind shear will advect the accumulated condensation warming away from the disturbance center, which inhibits the further decrease of surface pressure and more intense cumulus convection.

The next environmental parameter examined is the low-level large-scale convergence, computed from the 20-day low-pass filtered wind field. The 850-hPa divergence field (Fig. 6c) shows that convergences appear primarily in the central and southern parts of the domain for the developing disturbances. The developing cases possess stronger convergences than the nondeveloping cases. Another variable we examined is the horizontal cyclonic shear, which has been linked in previous studies to the development of tropical disturbances (Burpee 1972; Rennick 1976; Norquist et al. 1977; Thorncroft and Hoskins 1994a,b; Wang and Chan 2002; Hsieh and Cook 2007). The composites of the 850-hPa horizontal cyclonic shear for both the developing and nondeveloping disturbances have negative values in the middle and

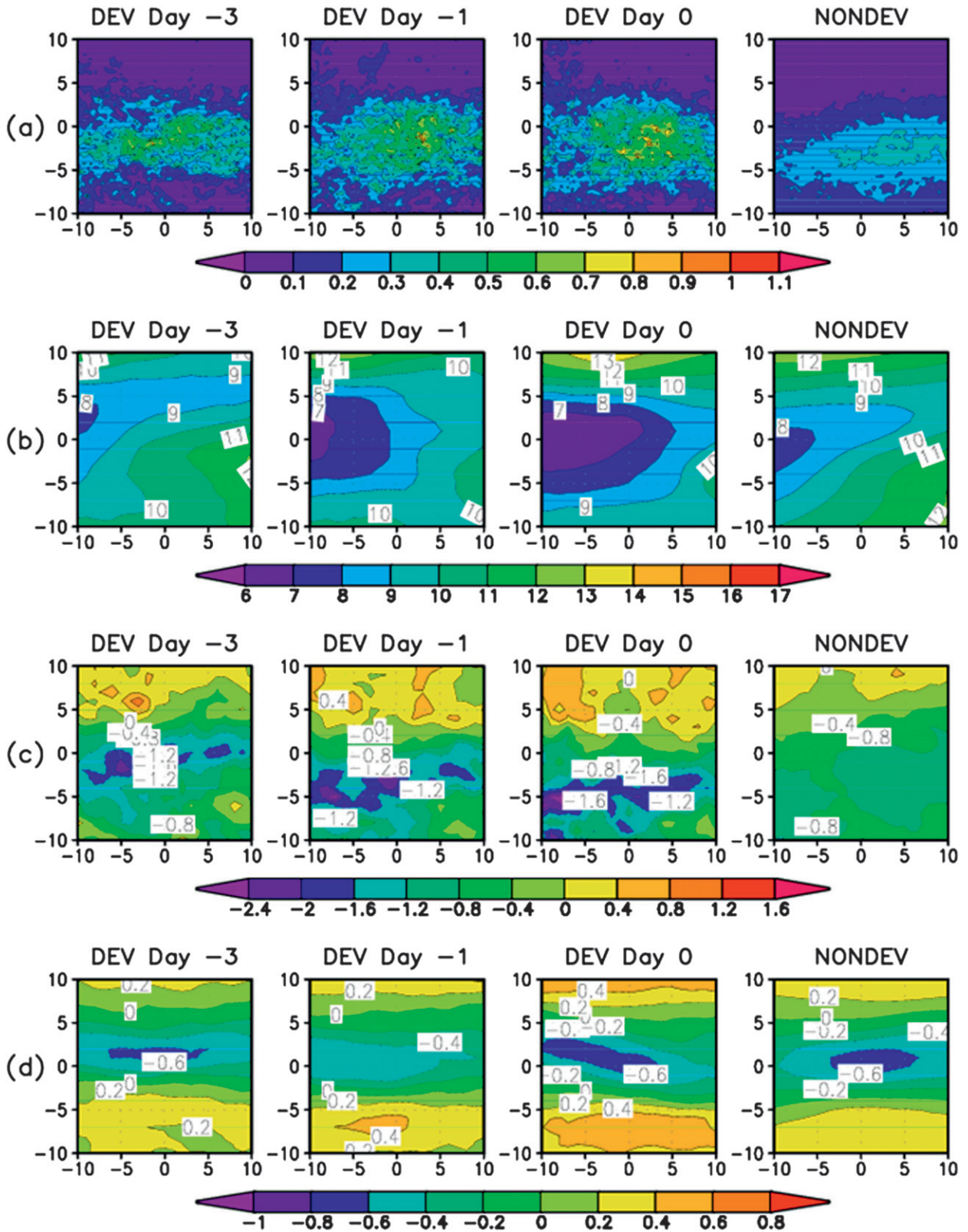


FIG. 6. Composite fields for developing and nondeveloping disturbances in the NATL. (a) Rain rate (mm hr^{-1}), (b) speed of 20-day low-pass filtered wind shear vector between 200 and 850 hPa (m s^{-1}), (c) 20-day low-pass filtered 850-hPa divergence (10^{-6} s^{-1}), and (d) 20-day low-pass filtered 850 hPa $\partial u/\partial y$ (10^{-5} s^{-1}). For all the composite fields, the horizontal-vertical axis measures relative longitudinal-latitude distance in degrees from the center.

TABLE 2. The duration time of nondeveloping disturbances in the NATL and the WNP.

No. of cases	No. of days										Tot
	3	4	5	6	7	8	9	10	11	>11	
NATL	21	18	20	10	8	11	9	4	5	2	108
WNP	14	18	10	12	7	4	4	3	4	2	78

positive values to the north and south (Fig. 6d). The magnitude of the cyclonic shear for developing disturbances at day -3 is comparable to that of the nondeveloping disturbances. The developing disturbances have weakening horizontal shear at day -2 and -1 , and then it intensifies again by day 0. Its vertical profile and importance to TC genesis will be examined further later.

c. Vertical profiles of zonal wind, cyclonic shear, and specific humidity

Whether a tropical disturbance will develop or not also depends on its vertical structure and the vertical profile of the ambient environment. Many previous studies have demonstrated that a small vertical shear between 200 and 850 hPa is favorable for TC formation. This conclusion is also supported by Fig. 6b. We plotted the vertical profile of a 20-day low-pass filtered zonal wind (Fig. 7) for the $20^\circ \times 20^\circ$ domain average of the developing and nondeveloping composites. It is interesting to note that for both the developing and nondeveloping disturbance composites, an easterly shear always appears between 1000 and 600 hPa and a westerly shear always appears between 600 and 200 hPa. Because of this change of direction of the shear, the conventionally defined vertical shear between 850 and 200 hPa may not be the best choice to distinguish an environmental condition favorable for TC genesis. As illustrated by the thick black line in Fig. 7, the vertical shear of the zonal flow between 850 and 200 hPa from day -3 to -1 is either close to or greater than that in the nondeveloping composite. A much better distinguishing vertical shear is between 1000 and 600 hPa (the dashed black line in Fig. 7). Note that at day -3 , the developing disturbances even possess a slightly smaller 1000–600-hPa vertical shear (-3.21 m s^{-1}) than the nondeveloping disturbances (-3.62 m s^{-1}). The shear decreases from day -3 to -1 . At day -1 , the 1000–600-hPa shear is -2.25 m s^{-1} , which is only 62% of that of the nondeveloping composite. Thus, the vertical shear between 1000 and 600 hPa is a better parameter to identify a TC-genesis-favoring environment in the NATL, keeping in mind that our analysis always follows the disturbances even though we are examining the large-scale pattern with wavelength greater than 6000 km.

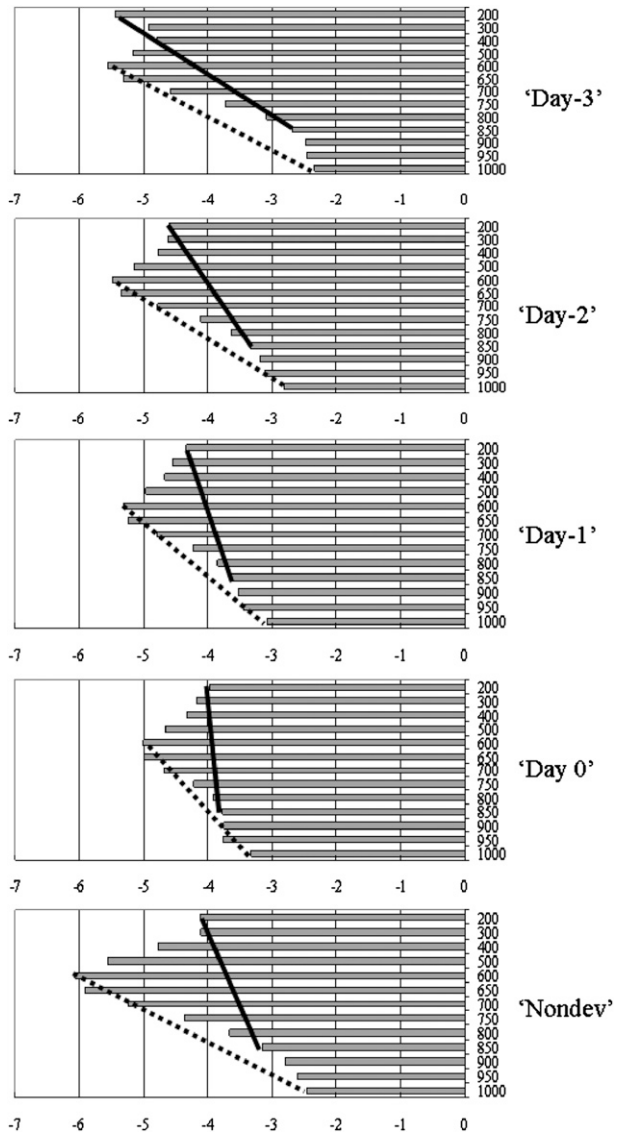


FIG. 7. Vertical profiles of $10^\circ \times 10^\circ$ domain-averaged composites of 20-day low-pass filtered zonal wind for developing and nondeveloping disturbances in the NATL (m s^{-1}). The solid and dashed lines mark 850–200- and 1000–600-hPa vertical shear, respectively.

As shown in Fig. 6d, horizontal wind shear changes sign at some distance from the center of the disturbance in the north–south direction, suggesting that barotropic instability may play a role in the growth of the disturbance. However, when taking a total domain average of Fig. 6d, the positive shear region in the outer part of the domain would reduce the intense shear in the central part of disturbances. To eliminate this artifact, we take a smaller domain from -5° to 5° in the north–south direction when computing the domain average (a box of size $20^\circ \times 10^\circ$). The vertical profile of the domain

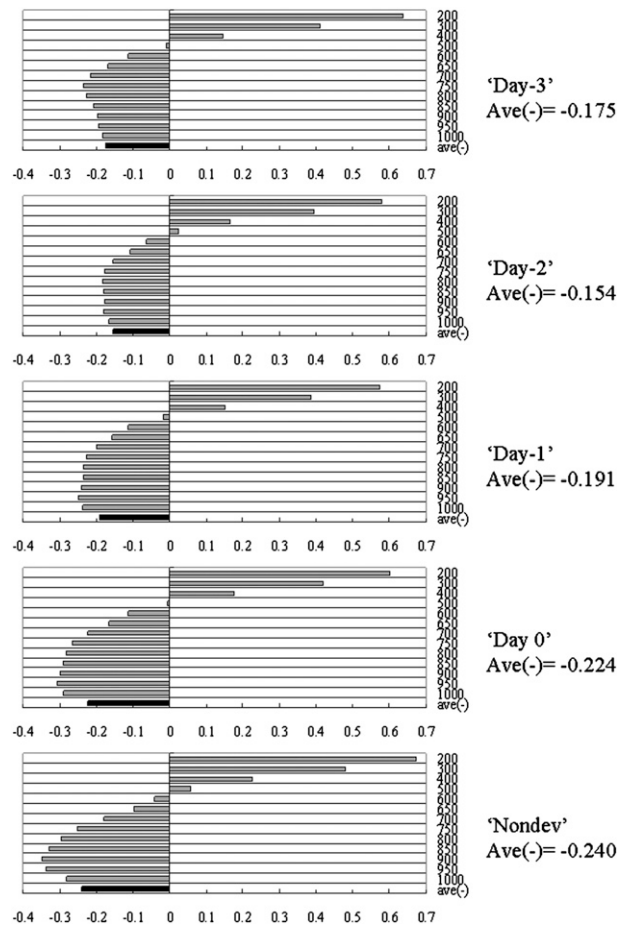


FIG. 8. Vertical profiles of $20^{\circ} \times 10^{\circ}$ domain-averaged composites of 20-day low-pass filtered $\partial u/\partial y$ (10^{-5} s^{-1}) for developing and nondeveloping disturbances in the NATL. The black bar in each panel represents vertical average of negative bars (averaged value is marked to the right of panel) at lower levels.

average of the horizontal wind shear ($\partial u/\partial y$) is shown in Fig. 8. Also note from Fig. 8 that $\partial u/\partial y$ is negative for the lower part of the domain and positive for the upper part. To identify the integrated effect of $\partial u/\partial y$, we take the vertical average of the horizontal average for levels with negative values only (roughly from 1000 to 500 hPa), plotted as the lowest bar in Fig. 8 for each group. The overall horizontal shear at day -3 and -2 are smaller than the one for the nondeveloping group. It then increases at day -1 and 0 and becomes comparable to the nondeveloping one.

Figure 9 depicts the vertical profile of the horizontal domain average of the divergence. Note that large convergence exists at low levels within the boundary layer. There are large variations in the vertical within each frame. We compute the vertical averages of the low-level divergence (with negative sign) and plot them as the last bar at the bottom of each frame. Even though the

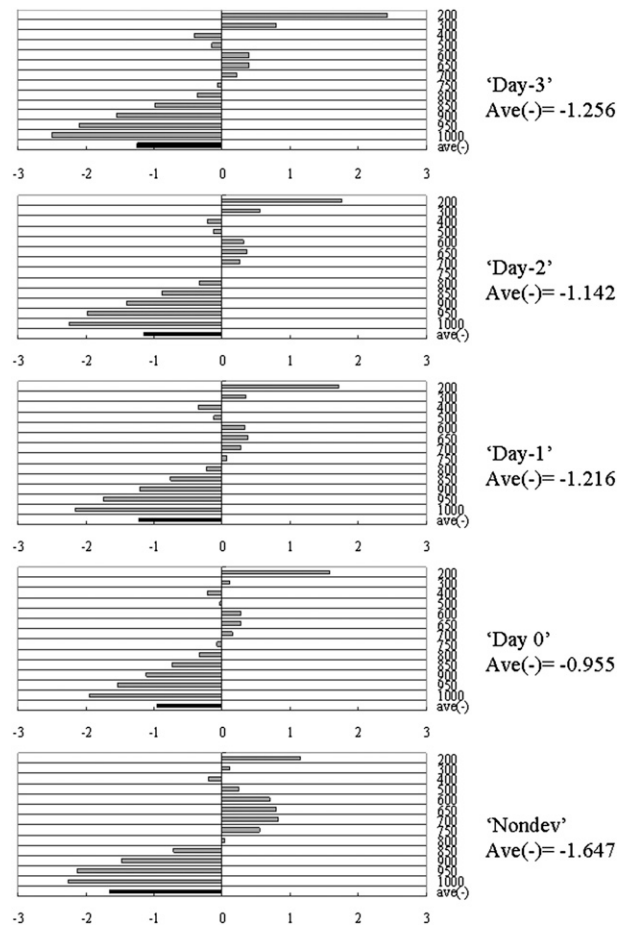


FIG. 9. Vertical profiles of $10^{\circ} \times 10^{\circ}$ domain-averaged composites of 20-day low-pass filtered divergence (10^{-6} s^{-1}) for developing and nondeveloping disturbances in the NATL. The black bar in each panel represents vertical average of negative bars (averaged value is marked to the right of panel) at lower levels.

nondeveloping group has a larger mean convergence than the developing group, it is not significant in distinguishing the two groups. But its importance changes as we examine the eastern and western Atlantic separately, which will be discussed later. This figure is shown to be compared with its counterpart in the WNP in Part II.

Figures 10a,b show the vertical distribution of the domain-averaged specific humidity difference fields between the developing and the nondeveloping group in two different domain sizes ($20^{\circ} \times 20^{\circ}$ and $10^{\circ} \times 10^{\circ}$). A positive difference appears throughout the troposphere, implying that the developing disturbances have larger specific humidity at each level. The specific humidity difference attains a maximum value near the surface and decreases with height. While a marked difference with the nondeveloping composite exists, the humidity difference among the developing composites from day -3 to 0 is small.

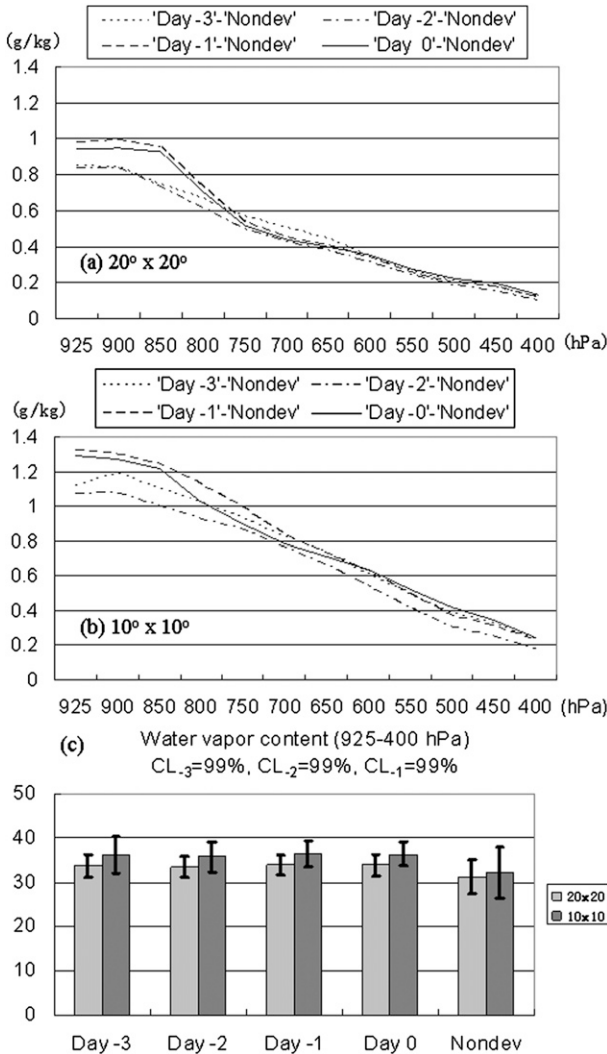


FIG. 10. Difference of domain-averaged specific humidity between the developing and nondeveloping disturbances at different vertical levels: (a) in a $20^\circ \times 20^\circ$ domain, (b) in a $10^\circ \times 10^\circ$ domain, and (c) domain-averaged ($20^\circ \times 20^\circ$ in light gray, $10^\circ \times 10^\circ$ in dark gray) composite of water vapor content (925–400 hPa) (kg). CL-3, CL-2, and CL-1 denote the comparison of developing disturbances at day -3, -2, and -1, with nondeveloping disturbances statistically significant at confidential level 99%.

Given the fact that the specific humidity of developing disturbances are greater than that of nondeveloping disturbances at all levels from 925 to 400 hPa, we anticipated that the water vapor content between these two pressure layers would be a good parameter to differentiate between the developing and nondeveloping cases. Figure 10c shows the total water vapor content between 925 and 400 hPa for each of the developing and nondeveloping composites. Consistent with the results shown in Figs. 10a,b, the developing disturbances have greater water vapor content than the nondeveloping disturbances.

A two-sample *t* test is used to test the significance of the difference between the developing and nondeveloping groups. We found that the differences at day -3, -2, and -1 are all statistically significant and exceed the 99% confidence level.

4. Variability within each developing and nondeveloping group and a box difference index

In the previous section, we focused primarily on the mean composite difference between the developing and nondeveloping waves. To thoroughly understand the distinctive characteristics of the two groups of disturbances, we also need to examine the variability of the samples within each group. Using the standard deviation to measure the extent of sample spread, we calculate both the mean and standard deviation of the key variables we analyzed previously and plot them with a box-and-whiskers format.

Figure 11 shows the box-and-whiskers plots for the synoptic-scale relative vorticity, SST, 500-hPa relative humidity, rain rate, vertical wind shear, and low-level divergence fields. For each box and whisker, the horizontal lower and upper lines indicate total range, upper and lower limits of the box indicate mean plus/minus standard deviation, and the central line indicates mean. Except for Fig. 11a, which is for the maximum 3–8-day filtered relative vorticity within the $20^\circ \times 20^\circ$ box, all other variables are the averages in domain. For each variable, the differences of the standard deviations between the developing and nondeveloping samples are quite small, although the maximum and minimum of the samples vary widely. Using a two-sample *t* test, we calculate the statistical significance between the developing (day -3 through -1) and nondeveloping disturbances for each variable. As expected, the difference of 3–8-day filtered 850-hPa relative vorticity between the two groups does not pass the 95% confidence level (Fig. 11a), which is consistent with the comparison of the horizontal patterns in the previous section (Fig. 4a). The difference of 20-day low-pass filtered 850-hPa divergences also fails to pass the significance test (Fig. 11f). For the relative humidity, only day -3 passes the 99% confidence level significance test. At day -1, the domain-averaged relative humidity is less than that of day -3 because of a relatively dry region (with relative humidity less than 42%) in the northwest of the domain. The vertical shear decreases gradually as the genesis date approaches. The difference between the developing disturbances at day -1 and the nondeveloping cases passes the 99% confidence level significance test. As for SST (Fig. 11b) and rain rate (Fig. 11d), both the differences at day -3 and -1 passed the significance test with confidence levels of 99% and 95%, respectively.

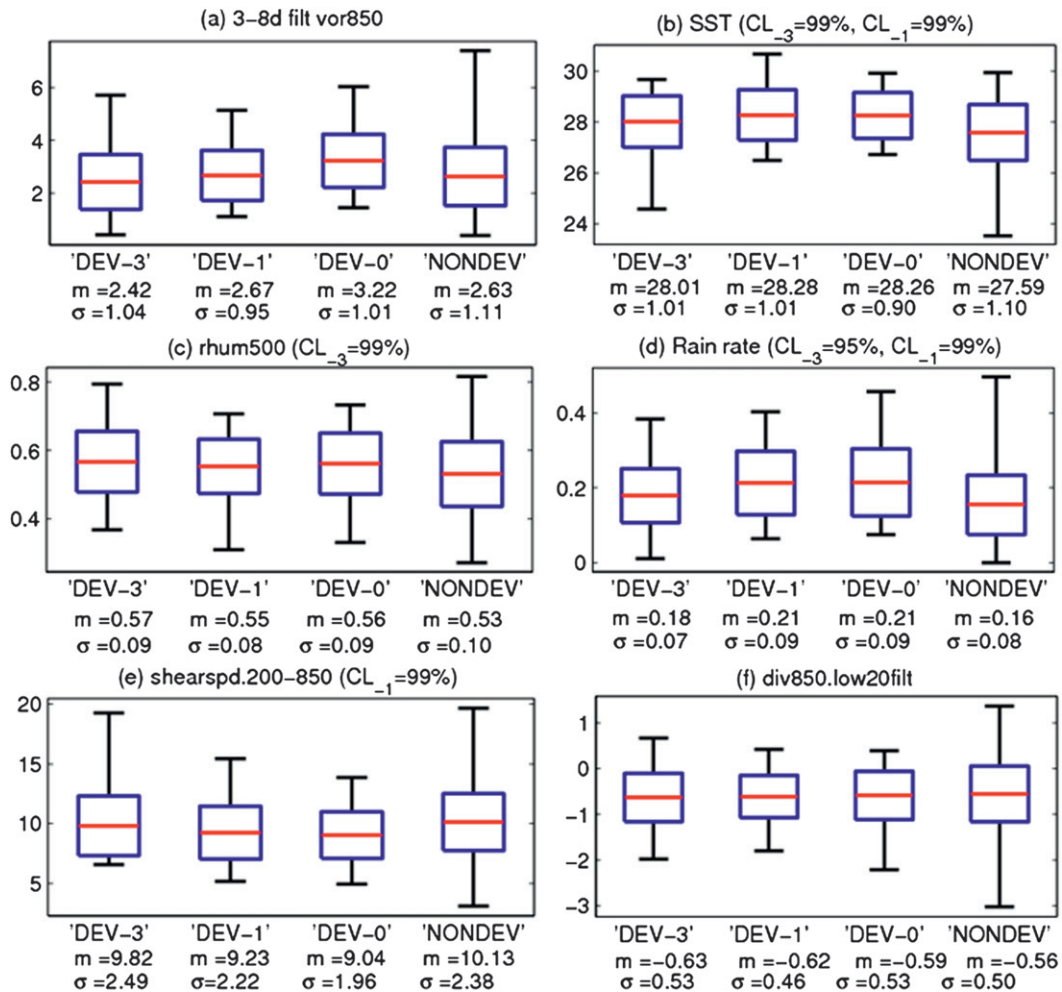


FIG. 11. Box-and-whiskers figures for (a) maximum 3–8-day filtered 850-hPa relative vorticity (10^{-5} s^{-1}) and $20^\circ \times 20^\circ$ box average, (b) SST ($^\circ\text{C}$), (c) 500-hPa relative humidity (%), (d) rain rate (mm hr^{-1}), (e) 20-day low-pass filtered vertical wind shear speed between 200 and 850 hPa (m s^{-1}), and (f) 20-day low-pass filtered 850-hPa divergence (10^{-6} s^{-1}). Mean is denoted by m (red line), and sigma denotes the standard deviation. A blue box depicts the variation between $m - \sigma$ and $m + \sigma$. Whiskers represent the minimum and maximum of the samples. CL₋₃ and CL₋₁ denote the comparison of developing disturbances at day -3 and -1 with nondeveloping disturbances statistically significant at confidential level 95% or 99%.

From both the scientific understanding and forecast application perspective, it is desirable to construct an objective parameter or index to quantitatively measure the difference. For this purpose, we introduce a box difference index (BDI). We give the index this name because it is associated with the box-and-whiskers figures. The definition of the index is as below:

$$\text{BDI} = \frac{M_{\text{DEV}} - M_{\text{NONDEV}}}{\sigma_{\text{DEV}} + \sigma_{\text{NONDEV}}},$$

where M_{DEV} and σ_{DEV} (M_{NONDEV} and σ_{NONDEV}) represent the mean and standard deviation of the variables for the developing (nondeveloping) cases. In this

study, we only focus on the discussion of the BDI feature at day -1. While the standard deviation is always positive, the mean can be positive or negative, depending on the physical property of the variable. Therefore, while the sign of the BDI reflects the physical nature of a variable, the magnitude of the BDI measures how well the variable can differentiate between the developing and nondeveloping disturbances. The greater the BDI amplitude is, the better a variable can be used to predict whether or not cyclogenesis will happen.

To illustrate what a BDI value means, we consider a special case of relative humidity in which the standard deviations of the developing and nondeveloping groups are same. Figure 12 shows what it looks like in

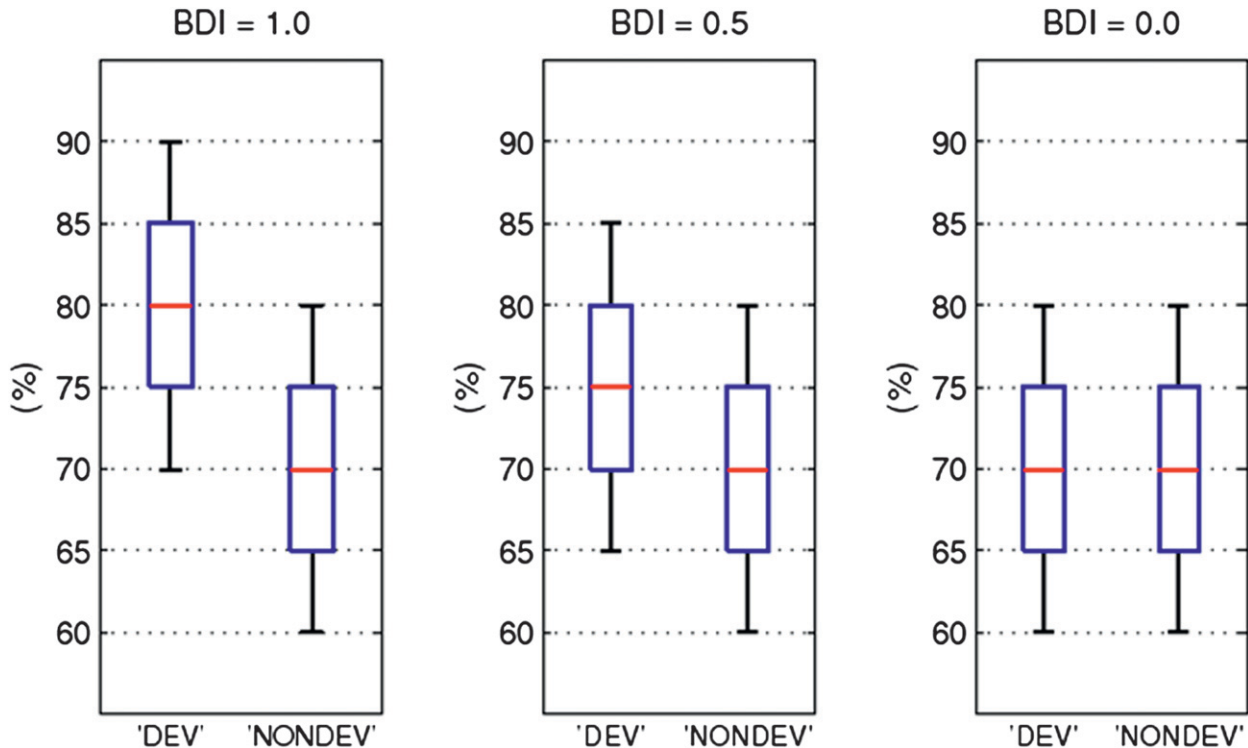


FIG. 12. Box-and-whiskers figure showing special cases of relative humidity where the BDI is 1, 0.5, and 0, respectively, for the developing and the nondeveloping group.

a box-and-whiskers figure when BDI is 0, 0.5, and 1. It is obvious that $BDI = 0$ implies there is no difference between the two groups. $BDI = 1$ denotes a case in which the developing and nondeveloping groups are well separated, whereas $BDI = 0.5$ implies that the two groups are partially separated.

While previous studies (e.g., Gray 1968, 1975; McBride and Zehr 1981) pointed out various parameters crucial for TC formation, the relative importance of these parameters is not clear. Camargo et al. (2007) studied the effect of ENSO on TC genesis and found that the changes of relative humidity and vertical shear primarily account for the decreased TC frequency in the Atlantic during the El Niño year, while the changes of relative humidity and vorticity are important for the eastward shift in the mean genesis location of TCs in the WNP. The results imply that the controlling parameters for TC genesis may be different at different basins. Even for the same parameter (say, relative humidity), it is not clear which level and what domain average of the parameter are most representative. With the aid of the BDI, we can objectively evaluate how important a variable is in terms of distinguishing the developing and nondeveloping disturbances. Using this objective method, it is possible to rank all relevant variables/parameters associated with TC genesis in each basin. The BDI can provide a basis

for predictor selection and for constructing statistical TC genesis forecast models.

To demonstrate the usefulness of the BDI, we will use relative vorticity as an example. It is well known that developing disturbances usually have a larger relative vorticity at lower levels, but it is not clear which level best represents the difference. Figure 13a shows the calculated BDIs for relative vorticity at different vertical levels in the NATL. A maximum BDI (0.32) occurs at 700 hPa, which suggests that the relative vorticity differences between the developing and nondeveloping disturbances are most significant at 700 hPa in the NATL, even though the maximum relative vorticity usually appears at a lower level (near the top of the boundary layer).

Figure 13b is another example that demonstrates the usefulness of the BDI. The variable we analyzed is the relative humidity. It is noted that for a $20^\circ \times 20^\circ$ domain, the area-averaged relative humidity BDI has a maximum value (0.4) at 800 hPa. With the reduction of the domain from a $20^\circ \times 20^\circ$ box to a $10^\circ \times 10^\circ$ box, the averaged relative humidity field has a larger BDI value (0.44) and the maximum BDI is located at 750 hPa. Thus, through this objective way, we can determine for each variable which level and what domain size are best to show the difference between the developing and nondeveloping cases.

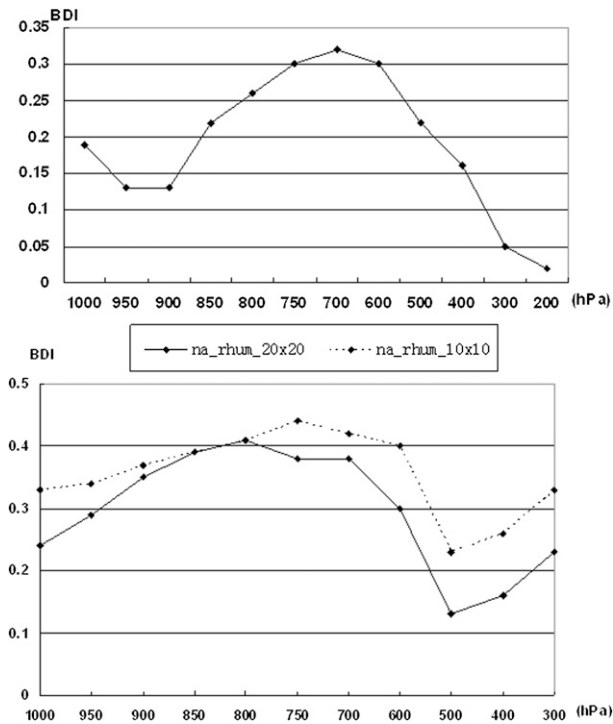


FIG. 13. (top) BDI for maximum relative vorticity at different levels, and (bottom) BDI for relative humidity averaged with different domain size at different levels.

The rank of the key variables based on their BDI values for the NATL is sorted in Table 3. Because time filtering cannot be applied in real-time TC genesis forecast, in the table we only list the BDIs for unfiltered variables. Note that the water vapor content from 925 to 400 hPa ranks at the top of all the parameters; the second parameter is rain rate, and SST follows as the third most important parameter. For parameters that can be calculated at different vertical levels, we only list the maximum BDI among all the vertical levels. For example, the relative vorticity parameter has a maximum BDI (0.32) at 700 hPa, but its BDI at 600/750 hPa is also large (0.30). Nevertheless, only BDI of the maximum relative vorticity at 700 hPa is listed. Also, because the 925–400-hPa water vapor content parameter generally represents an overall effect of the moisture field, we exclude relative humidity at individual levels from our list to prevent from overlapping. Among the parameters we calculated, vertically averaged horizontal divergence has the smallest BDI (−0.03). As one can see from this table, vorticity, horizontal shear, and vertical shear parameters all appear in the lower half of the table. Based on the BDI results, we propose that moisture is the most important factor when attempting to separate developing disturbances from nondeveloping ones in the NATL, and dynamic parameters might be of secondary importance.

TABLE 3. Ranks of key genesis parameters in the NATL and their corresponding BDI values (sign and magnitude).

Variable name	BDI	
	Sign	Magnitude
925–400-hPa water vapor content ($10^\circ \times 10^\circ$)	+	0.49
Rain rate ($20^\circ \times 20^\circ$)	+	0.35
SST ($20^\circ \times 20^\circ$)	+	0.33
Max 700-hPa relative vorticity	+	0.32
1000–600-hPa vertical shear ($20^\circ \times 20^\circ$)	−	0.19
Translational speed	−	0.15
Vertically averaged $\partial u/\partial y$ ($20^\circ \times 10^\circ$)	−	0.13
Vertically averaged divergence ($20^\circ \times 20^\circ$)	−	0.03

5. Geographic dependence

Using the BDI analysis, we identified key parameters that distinguish the developing disturbances from the nondeveloping disturbances in North Atlantic. As shown in the composite samples distribution (Fig. 3), the developers are more populated over the west Atlantic while the nondevelopers are more populated over the east Atlantic. It is well known that the large-scale environmental conditions (e.g., wind, SST, and moisture) between the west and east Atlantic are quite different. The former region has more favorable environmental conditions for TC formation than the latter. Thus the key genesis parameters may depend on the geographical location in the Atlantic.

To explore the geographic dependence, we performed the similar BDI calculations but separated the samples into two regions: the west and east Atlantic (separated by 40°W). Table 4 shows the BDI results for these two subbasins. While the top parameter remains the same, the ranks of other parameters do change from west to east Atlantic. The SST and maximum vorticity at 700 hPa still have higher importance in the east Atlantic, while the SST becomes less important and the vertically averaged horizontal shear and horizontal divergence becomes more important in the west Atlantic. This is understandable as TC genesis is more (less) sensitive to SST in regions where the mean SST is relatively low (high). The most striking difference between the west and east Atlantic is the change of the BDI for the integrated divergence (the low-level convergence only). In the total NATL domain, the BDI is only (−) 0.03, while it increases to (−) 0.39 in the western NATL and changes to (+) 0.08 in the eastern NATL. These differences further enhance the importance of thermodynamic control in the east Atlantic and bring up some importance of dynamic control in the west Atlantic.

Figure 7 shows the decrease of the easterly wind shear from day −3 to 0. To examine how this feature depends on the geographic location, we checked the environmental

TABLE 4. List of the BDI values of key genesis parameters in the west and east Atlantic (sign and magnitude).

Variable name	West	East
925–400-hPa water vapor content ($10^\circ \times 10^\circ$)	0.48	0.53
Rain rate ($20^\circ \times 20^\circ$)	0.48	0.35
SST ($20^\circ \times 20^\circ$)	0.20	0.40
Max 700-hPa relative vorticity	0.28	0.38
1000–600-hPa vertical shear ($20^\circ \times 20^\circ$)	–0.09	0.00
Translational speed	–0.13	–0.11
Vertically averaged $\partial u/\partial y$ ($20^\circ \times 10^\circ$)	–0.27	–0.10
Vertically averaged divergence ($20^\circ \times 20^\circ$)	–0.39	0.08

vertical shear effect in the west and east Atlantic separately. It is noted that the decreasing trend of the easterly shear between 600 and 1000 hPa as the genesis approaches from day –3 to 0 was found in both the regions. The only difference is that in east Atlantic the vertical shear between 1000 and 600 hPa is always an easterly shear, while in the west Atlantic, the vertical shear changes from a weak easterly shear at day –3 to a weak westerly shear at day 0 (Figures not shown). This is likely due to the change of the mean flow that disturbances experience as they propagate from east to west as the midlevel easterly jet gradually changes to the low-level trade wind from the east Atlantic to the west Atlantic. As shown in Table 4, the BDI suggests that in a smaller region of east or west part of Atlantic, the shear between 1000 and 600 hPa can't be used to differentiate developing disturbances from nondeveloping disturbances as they are both very small. This is also likely due to the change of shear direction that would not be identified by a single magnitude of the shear between fixed levels. Our findings that lower tropospheric shear cannot distinguish developing and nondeveloping disturbances are also consistent with the results from Dunkerton et al. (2009). More research remains to be carried out on this.

For both the developing and nondeveloping cases, the analysis follows the propagation of the disturbance in a “Lagrangian” manner similar to that advocated by Dunkerton et al. (2009). An issue related to this analysis is how to determine a precise boundary for the disturbance vortex. In our composite and BDI analyses, we usually use a relatively large domain size: either a $20^\circ \times 20^\circ$, $20^\circ \times 10^\circ$, or $10^\circ \times 10^\circ$ box. The reason we used a larger domain is to primarily examine key environmental conditions under which the disturbances evolve. To examine the sensitivity of the result to the domain size, we calculated the BDI values with a smaller box size ($4^\circ \times 4^\circ$). Our new calculations with a smaller domain show that BDIs are different for some of the parameters. For example, in the North Atlantic, the BDI magnitude for 925–400-hPa water vapor content is 0.49 for a $10^\circ \times 10^\circ$ box, and increases to 0.51 when we use

TABLE 5. List of the BDI magnitude for 925–400-hPa water vapor content and vertically averaged divergence with different box size.

Parameters	Box size		
	$20^\circ \times 20^\circ$	$10^\circ \times 10^\circ$	$4^\circ \times 4^\circ$
925–400-hPa water vapor content	0.43	0.49	0.51
Vertically averaged divergence	0.03	0.11	0.02

a $4^\circ \times 4^\circ$ box (Table 5). For vertically averaged divergence, the BDI magnitude is 0.03 for a $20^\circ \times 20^\circ$ box, but increases to 0.11 when using a $10^\circ \times 10^\circ$ box, and decreases to 0.02 when using a $4^\circ \times 4^\circ$ box. The result above suggests that the selection of the box size is parameter dependent. A larger domain should be selected for large-scale environmental parameters, while for some parameters that reflect the wave characteristics, a smaller size box should be selected.

6. Impact of upstream winds on TC genesis

Previous studies suggested a close relationship between the SAL and the downstream TC activity (Dunion and Veldon 2004; Wu et al. 2006). It was proposed that SAL generally influences TC formation in three ways (Dunion and Veldon 2004). First, it enhances the temperature inversion to inhibit the occurrence of convection; second, it entrains more dry air into the TC circulation; and lastly, it increases the vertical shear. The dry airs in SAL are either associated with the outbreaks of the dust from Africa or with the midlatitude subsidence. Carlson and Prospero (1972) documented that the dust airs have a desert origin and are related to a series of large-scale anticyclonic eddies moving westward over the tropical Atlantic above the trade wind moist layer. Braun (2010) demonstrated that the dry airs to the north of the AEWs are most likely associated with large-scale subsidence. As very dry airs with high concentrated dust in SAL are associated with strong easterly wind over West Africa, we hypothesize that when the easterly wind over West Africa becomes stronger, more dust will be entrained into SAL, resulting in the decrease of the local relative humidity. To test our hypothesis, we examined the relationship between the relative humidity over the major TC development region off the African coast and the easterly wind over the African continent. Figure 14 shows a significant negative lagged correlation between the downstream relative humidity and the upstream 650-hPa easterly wind for the period of 2004–08. For each year, the maximum lagged correlation occurs at day –1. While there is a small year-to-year variation, the significant correlation regions and the amplitude of the correlation coefficients remain

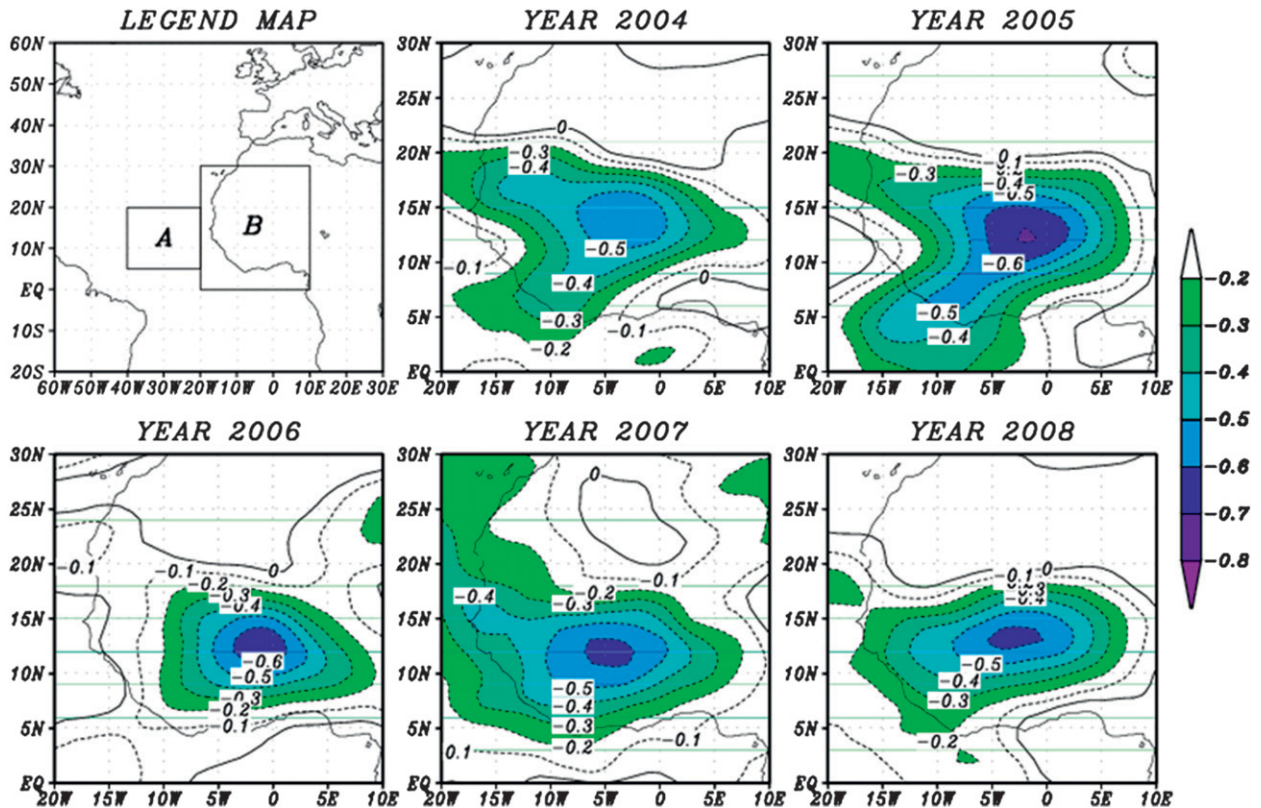


FIG. 14. Correlation map between averaged 850-hPa relative humidity (%) in box “A” and 650-hPa easterly wind in box “B” (1-day lag). Only negative correlation is displayed. Correlation passed 95% confidential level is shaded.

stable. Figure 14 also shows that the maximum lagged correlation coefficient for each year is in the range of 0.6–0.7, with the maximum center appearing in the region of (10°–15°N, 0°–5°W). The lagged correlation at day -2 and -3 is much weaker compared to that at day -1 (figures not shown). The results shown in Fig. 14 support our previous hypothesis.

7. Summary and conclusions

Substantial improvements in satellite retrievals, data assimilation, and numerical models in recent decades have made global atmospheric analysis closer to reality (Peng et al. 2004; Baker et al. 2005). With the use of global analysis, we identify important parameters that control the development of tropical disturbances to form tropical cyclones following individual disturbances. This study obtains a more comprehensive picture of why some tropical disturbances formed TCs while others didn't. Part I of this report focuses on Atlantic cases and Part II focuses on the western North Pacific cases.

A comparison of the distinguishing characteristics of nondeveloping disturbances and developing disturbances is summarized in Table 6. First, a fast-moving disturbance

is less likely to form a TC than a slower-moving disturbance. A disturbance with a slower translational speed can reside in a TC-favorable environment longer to allow for vigorous convections to occur with sustained precipitation. Developing disturbances have the following characteristics: slower translational speed, larger moisture content, higher SST, and smaller vertical shear between 1000 and 600 hPa. The SST distribution also shows a seasonal influence on TC genesis, as its occurrence peaks in September when the subtropical high shifts to the east and local SST reaches its maximum.

While most of the parameters examined show statistical significant differences between developing and nondeveloping disturbances, it is not clear what parameters are more important than others. An index (BDI) is introduced to objectively and quantitatively identify leading parameters that distinguish developing and nondeveloping disturbances. This index includes both the mean and standard deviation of the data samples within each developing and nondeveloping group. The BDI can be used to assess the relative importance of key dynamic and thermodynamic variables in determining the outcome of a tropical disturbance for TC formation. Based on the BDIs computed, we obtained a set of

TABLE 6. Summarized differences between developing cases and nondeveloping cases in the NATL.

	Developing	Nondeveloping
Translational speed	Slow	Fast
SST	High	Low
Rainfall	Intense	Weak
Vertical shear	Weak	Strong
925–400-hPa water vapor content	High	Low

parameters that are optimal in distinguishing the developing and nondeveloping disturbances in the NATL. According to our results, it is suggested that the 925–400-hPa moisture content, rain rate, and SST are the most important parameters, followed by 700-hPa maximum relative vorticity, 1000–600-hPa vertical shear, the translational speed, and vertically averaged horizontal shear for determining whether or not a tropical Atlantic disturbance will develop into a TC. These analyses indicate that thermodynamic variables play more important roles than dynamic variables in controlling the formation of TCs in the North Atlantic.

When we examine the geographic difference between the west and east Atlantic (separated by 40°W), the 925–400-hPa integrated water vapor remains as the most important parameter for both regions. The SST and maximum vorticity at 700 hPa still have higher importance in the east Atlantic, while SST becomes less important and the vertically averaged horizontal shear and horizontal divergence become more important in the west Atlantic. This difference further enhances the importance of thermodynamic control in the east Atlantic and highlights some importance of dynamic control in the west Atlantic. The ranking of these parameters provides an important basis for finding the best predictors for constructing a statistical TC formation forecast model.

While our findings are consistent with other studies in a broad sense regarding the controlling factors for TC genesis, our study points to a more precise order of importance among these parameters and also to regions and vertical domains that one could look into. Note that a model such as NOGAPS has bias in its forecast and analysis fields. Hodges et al. (2003) documented difference between NCEP–National Center for Atmospheric Research (NCAR) reanalysis and ECMWF reanalysis. Therefore, caution is needed in interpreting the analysis result because of uncertainty in the NOGAPS analysis field. Our study is also based on a limited number of sampling years that may also impact our results. This needs to be verified with future studies by including more data and different model analysis such as the NCEP and ECMWF reanalysis.

Acknowledgments. We thank Drs. Thorncroft and Dunkerton and another anonymous reviewer for their valuable comments and constructive suggestions. We also thank Ms. May Izumi for her editorial service. This study was supported by ONR Grants N000140810256 and N000141010774, NRL Subcontract N00173-06-1-G031, and the International Pacific Research Center, which is sponsored by the Japan Agency for Marine–Earth Science and Technology (JAMSTEC), NASA (Grant NNX07AG53G), and NOAA (Grant NA17RJ1230).

REFERENCES

- Anthes, R. A., Ed., 1982: *Tropical Cyclones: Their Evolution, Structure and Effects*. Meteor. Monogr., No. 41, Amer. Meteor. Soc., 208 pp.
- Avila, L. A., 1991: Atlantic tropical systems of 1990. *Mon. Wea. Rev.*, **119**, 2027–2033.
- , and R. J. Pasch, 1995: Atlantic tropical systems of 1993. *Mon. Wea. Rev.*, **123**, 887–896.
- Baker, N. L., T. F. Hogan, W. F. Campbell, R. L. Pauley, and S. D. Swadley, 2005: The impact of AMSU-A radiance assimilation in the U.S. Navy's Operational Global Atmospheric Prediction System (NOGAPS). NRL Memo. Rep. NRL/MR/7530-05-8836, 18 pp. [Available from the Naval Research Laboratory, 7 Grace Hopper Ave., Monterey, CA 93943-5502.]
- Berry, G., C. Thorncroft, and T. Hewson, 2007: African easterly waves during 2004—Analysis using objective techniques. *Mon. Wea. Rev.*, **135**, 1251–1267.
- Braun, S. A., 2010: Reevaluating the role of the Saharan air layer in Atlantic tropical cyclogenesis and evolution. *Mon. Wea. Rev.*, **138**, 2007–2037.
- Burpee, R., 1972: The origin and structure of easterly waves in the lower troposphere of North Africa. *J. Atmos. Sci.*, **29**, 77–90.
- Camargo, S. J., K. A. Emanuel, and A. H. Sobel, 2007: Use of a genesis potential index to diagnose ENSO effects on tropical cyclone genesis. *J. Climate*, **20**, 4819–4834.
- Carlson, T. N., 1969: Synoptic histories of three African disturbances that developed into Atlantic hurricanes. *Mon. Wea. Rev.*, **97**, 256–276.
- , and J. M. Prospero, 1972: The large-scale movement of Saharan air outbreaks over the northern equatorial Atlantic. *J. Appl. Meteor.*, **11**, 283–297.
- Christiano, J., and T. J. Fitzgerald, 2003: The band pass filter. *Int. Econ. Rev.*, **44**, 435–465.
- DeMaria, M., 1996: The effect of vertical shear on tropical cyclone intensity change. *J. Atmos. Sci.*, **53**, 2076–2088.
- , J. A. Knaff, and B. H. Connell, 2001: A tropical cyclone genesis parameter for the tropical Atlantic. *Wea. Forecasting*, **16**, 219–233.
- Diedhiou, A., S. Janicot, A. Vitard, P. Felice, and H. Laurent, 1999: Easterly wave regimes and associated convection over West Africa and tropical Atlantic: Results from the NCEP/NCAR and ECMWF reanalysis. *Climate Dyn.*, **15**, 795–882.
- Dunion, J. P., and C. S. Velden, 2004: The impact of the Saharan Air Layer on Atlantic tropical cyclone activity. *Bull. Amer. Meteor. Soc.*, **85**, 353–365.
- Dunkerton, T. J., M. T. Montgomery, and Z. Wang, 2009: Tropical cyclogenesis in a tropical wave critical layer: Easterly waves. *Atmos. Chem. Phys.*, **9**, 5587–5646.

- Erickson, S. L., 1977: Comparison of developing vs. non-developing tropical disturbances. Colorado State University Department of Atmospheric Science Paper 274, 89 pp.
- Frank, N. L., 1972: Atlantic tropical systems of 1971. *Mon. Wea. Rev.*, **100**, 268–275.
- Frank, W. M., and P. E. Roundy, 2006: The role of tropical waves in tropical cyclogenesis. *Mon. Wea. Rev.*, **134**, 2397–2417.
- Franklin, J. L., 2008: 2007 National Hurricane Center forecast verification report. NOAA/NWS/NCEP/Tropical Prediction Center Rep., 68 pp.
- Fu, B., T. Li, M. S. Peng, and F. Weng, 2007: Analysis of tropical cyclogenesis in the western North Pacific for 2000 and 2001. *Wea. Forecasting*, **22**, 763–780.
- , M. S. Peng, T. Li, and D. E. Stevens, 2012: Developing versus nondeveloping disturbances for tropical cyclone formation. Part II: Western North Pacific. *Mon. Wea. Rev.*, **140**, 1067–1080.
- Gray, W. M., 1968: A global view of the origin of tropical disturbances and storms. *Mon. Wea. Rev.*, **96**, 669–700.
- , 1975: Tropical cyclone genesis. Colorado State University Department of Atmospheric Science Paper 234, 121 pp.
- Grist, J. P., 2002: Easterly waves over Africa. Part I: The seasonal cycle and contrasts between wet and dry years. *Mon. Wea. Rev.*, **130**, 197–211.
- Hall, N. M. J., G. N. Kiladis, and C. D. Thorncroft, 2006: Three-dimensional structure and dynamics of African easterly waves. Part II: Dynamical modes. *J. Atmos. Sci.*, **63**, 2231–2245.
- Hodges, K. I., B. J. Hoskins, J. Boyle, and C. Thorncroft, 2003: A comparison of recent reanalysis datasets using objective feature tracking: Storm tracks and tropical easterly waves. *Mon. Wea. Rev.*, **131**, 2012–2037.
- Hopsch, S. B., C. D. Thorncroft, K. Hodges, and A. Aiyer, 2007: West African storm tracks and their relationship to Atlantic tropical cyclones. *J. Climate*, **20**, 2468–2483.
- , —, and K. R. Tyle, 2010: Analysis of African easterly wave structures and their role in influencing tropical cyclogenesis. *Mon. Wea. Rev.*, **138**, 1399–1419.
- Hsieh, J. S., and K. H. Cook, 2007: A study of the energetics of African easterly waves using a regional climate model. *J. Atmos. Sci.*, **64**, 421–440.
- Landsea, C. W., 1993: A climatology of intense (or major) Atlantic hurricanes. *Mon. Wea. Rev.*, **121**, 1703–1713.
- , G. D. Bell, W. M. Gray, and S. B. Goldenberg, 1998: The extremely active 1995 Atlantic hurricane season: Environmental conditions and verification of seasonal forecasts. *Mon. Wea. Rev.*, **126**, 1174–1193.
- Lau, K. H., and N. C. Lau, 1990: Observed structure and propagation characteristics of tropical summertime synoptic scale disturbances. *Mon. Wea. Rev.*, **118**, 1888–1913.
- McBride, J. L., and R. Zehr, 1981: Observational analysis of tropical cyclone formation. Part II: Comparison of non-developing versus developing systems. *J. Atmos. Sci.*, **38**, 1132–1151.
- Norquist, D. C., E. E. Recker, and R. J. Reed, 1977: The energetics of African wave disturbances as observed during phase III of GATE. *Mon. Wea. Rev.*, **105**, 334–342.
- Paradis, D., J.-P. Lafore, J.-L. Redelsperger, and V. Balaji, 1995: African easterly waves and convection. Part I: Linear simulations. *J. Atmos. Sci.*, **52**, 1657–1679.
- Peng, M. S., J. A. Ridout, and T. F. Hogan, 2004: Recent modifications of the Emanuel convective scheme in the Naval Operational Global Atmospheric Prediction System. *Mon. Wea. Rev.*, **132**, 1254–1268.
- Rennick, M. A., 1976: The generation of African waves. *J. Atmos. Sci.*, **33**, 1955–1969.
- Simmons, A. J., 1977: A note on the instability of the African easterly jet. *J. Atmos. Sci.*, **34**, 1670–1674.
- Simpson, R. H., N. Frank, D. Shideler, and H. M. Johnson, 1968: Atlantic tropical disturbances, 1967. *Mon. Wea. Rev.*, **96**, 251–259.
- Tam, C.-Y., and T. Li, 2006: The origin and dispersion characteristics of the observed tropical summertime synoptic-scale waves over the western Pacific. *Mon. Wea. Rev.*, **134**, 1630–1646.
- Thorncroft, C., and K. Hodges, 2001: African easterly wave variability and its relationship to Atlantic tropical cyclone activity. *J. Climate*, **14**, 1166–1179.
- , and B. J. Hoskins, 1994a: An idealized study of African easterly waves. Part I: A linear view. *Quart. J. Roy. Meteor. Soc.*, **120**, 953–982.
- , and —, 1994b: An idealized study of African easterly waves. Part II: A nonlinear view. *Quart. J. Roy. Meteor. Soc.*, **120**, 983–1015.
- , N. M. J. Hall, and G. N. Kiladis, 2008: Three-dimensional structure and dynamics of African easterly waves. Part III: Genesis. *J. Atmos. Sci.*, **65**, 3596–3607.
- Wallace, J., and C. P. Chang, 1969: Spectrum analysis of large-scale wave disturbances in the tropical lower troposphere. *J. Atmos. Sci.*, **26**, 1010–1025.
- Wang, B., and J. C. L. Chan, 2002: How strong ENSO events affect tropical storm activity over the western North Pacific. *J. Climate*, **15**, 1643–1658.
- Wu, L., S. A. Braun, J. J. Qu, and X. Hao, 2006: Simulating the formation of Hurricane Isabel (2003) with AIRS data. *Geophys. Res. Lett.*, **33**, L04804, doi:10.1029/2005GL024665.
- Zehr, R. M., 1992: Tropical cyclogenesis in the western North Pacific. NOAA Tech. Rep. NESDIS 61, 181 pp.

Copyright of Monthly Weather Review is the property of American Meteorological Society and its content may not be copied or emailed to multiple sites or posted to a listserv without the copyright holder's express written permission. However, users may print, download, or email articles for individual use.